Computational Engineering and Physical Modeling 2-4 (2019) 38-57

Contents lists available at CEPM

Computational Engineering and Physical Modeling

Journal homepage: www.jcepm.com

Lattice Boltzmann Simulation of Fluid Flow and Heat Transfer through Partially Filled Porous Media

Sh. Hassan[1,2], T.A. Himika[1], Md.M. Molla[1,2*], F. Hasan[3]

1. Department of Mathematics and Physics, North South University, Dhaka-1229, Bangladesh
2. Center for Applied Scientific Computing (CASC), North South University, Dhaka-1229, Bangladesh
3. Department of Engineering & Physical Sciences, La Trobe University, Melbourne, VIC 3086, Australia

*Corresponding author: mamun.molla@northsouth.edu

https://doi.org/10.22115/CEPM.2020.200817.1070

ARTICLE INFO

Article history:
Received: 08 September 2019
Revised: 12 February 2020
Accepted: 18 February 2020

Keywords:
Lattice boltzmann method;
Porous media;
REV scale;
Natural convection;
Fluid flow;
Heat transfer.

ABSTRACT

The main aim of this work is to observe the fluid flow and heat transfer characteristics through porous media at the REV (Representative Elementary Volume) scale in an enclosed squared cavity using LBM (Lattice Boltzmann Method) instead of traditional FVM, FDM, or FEM. Results are generated by varying the porosity (ε = 0.4, 0.6, 0.9), and other dimensionless variables: Rayleigh number (Ra = 10^3, 10^4, 10^5, 10^6), and Darcy number (Da =10^{-2}, 10^{-3}). The enclosed cavity was considered to be half-filled with pore materials, with horizontal porous layer and vertical porous layer, these two cases are studied for all the considered parameters. The influence of the dimensionless parameters as well as porosity on the fluid flow and heat transfer characteristics has been discussed in detail along with the influence of the placement of the pore material inside the cavity. In the end, it is observed form the results that the nature of the flow and rate of the heat transfer are affected significantly by the Ra values, Da values, and porosity level. The placement differences of the pore materials further shows differences in the fluid flow and heat transfer characteristics. A new and simpler forcing term for the porous media is used. This study can be useful while using a porous media in numerical designs and experimental designs. Fortran 90 is used for numerical simulations.

How to cite this article: Hassan S, Himika TA, Molla MM, hasan F. Lattice Boltzmann Simulation of Fluid Flow and Heat Transfer through Partially Filled Porous Media. Comput Eng Phys Model 2019;2(4):38–57. https://doi.org/10.22115/cepm.2020.200817.1070

1. Introduction

The importance of studying fluid flow considering a porous media and its heat transfer grabbed attention after researchers started to encounter theoretical and experimental discrepancies in applications like managing thermal distribution of any electronics cooling system, enhancement of heat transfer system, flow simulation etc. To computationally study fluid flow in porous materials and its heat transfer characteristics, many researchers relied on conventional simulation techniques like finite-difference[1,2], finite-volume [3–5] and finite-element methods [6,7], which are associated with discretization of macroscopic continuum equations. Therefore, the requirement of an accurate tool for simulating at microscopic level is still required.

Lattice Boltzmann Method (LBM), an alternative simulation technique, is relevant to both microscopic and macroscopic levels since it considers the behaviour of a group of fluid particles as one single unit. The LGA (Lattice Gas Automata), the origin of the LB-method, was initially used to numerically study fluid flow through porous media in the 1980s at different scales [8,9]. Flows in porous media can be classified in three scales namely: pore scale; REV scale; and; domain scale [10]. The REV scale is characterized as a least component and it is highly suitable for a porous flow, and domain scale>>REV scale>>pore scale [11]. The advantages of LBM are due to its simplicity and accuracy. Since LBM is the combination of microscopic model together with the mesoscopic kinetic equations of fluids, the kinetic characteristics of the method and elaborate bounce-back conditions for no-slip boundary condition makes it easier to design fluid flow considering a porous media in CFD studies. LBM is flexible to implement for rather composite designs, and has been a popular approach among the researchers to study multi-phase/multi-component fluid flows. The simulation technique was found to be less time-consuming and more accurate than some classical simulation methods as LBM does not require solving Laplace formulation of all computational Time-Steps to suit continuity equation for transient and incompressible flows, but it's essential to solve Navier-Stokes equation [12,13].

Numerical simulation of flows and heat transfer considering porous mediums requires solution of certain equations. Earlier, Darcy's equation had normally been utilized by research communities, but for fluid flows with high velocities, experimental data weren't found to be in accord with the theoretical prediction [14]. Therefore, the alterations were established by Forchheimer's equation [15,16] together with Brinkman's equation [17,18]. The Forchheimer's equation takes into account the influence of non-linear drags caused by solid matrix, whereas Brinkman's formulation involves viscous stresses led by solid boundaries. When the values of *Re* or *Da* is greater, non-linear drag coefficients have to be counted. On the other hand, Brinkman's alteration of the Darcy's formulation has substantial impact on the energy transportation method [14]. Therefore, combination of Brinkman and Forchheimer's equations can be considered as an appropriate approach for numerical study of flow and heat transfer considering a porous medium, which will resolve both viscous and inertial terms. Although the method is complicated it was found to be a good alternative predicting the heat transfer and fluid mechanism in the system which is considered to be non-Darcian [14,19,20]. The reliability of LBM to get adjusted into Brinkman-Forchheimer equation was earlier reported to be effective by some of the researchers

[14,21], but certain dimensionless parameters' assistance and influence should be mentioned here as well.

When exercising the fluid flow simulation considering a porous media, apart from LBM together with Brinkman-Forchheimer equation, three other dimensionless characters namely, *Ra*, *Nu*, and *Da* have to be valued. The *Ra* number describes the intensity of the fluid behaviour, *Nu* number is highly associated with the type of flow, either laminar (low *Nu*, close to *1*) or turbulent flow (high *Nu*, between *100-1000*), and *Da* number shows the relative impact of the permeability of the pore material against the cross-sectional area of this medium, i.e., squared of the diameter. Therefore, the values of those dimensionless parameters can describe the type or genre of fluid flow numerically, and thus the qualitative and quantitative performance of the simulations carried out in this paper can be truly evaluated.

In the light of above requirements and parameters, some of the relevant research works can be discussed here in brief. Tong and Subramanian [22] performed an analysis through rectangular enclosures partially filling with porous medium by finite-difference (FD) technique varying *Ra* number and *Da* number to show the influence of those dimensionless parameters. Although the results indicate the importance of squared cavity considering partially-filled porous medium to numerically study fluid flow and heat transfer, however, FD technique requires more computational times to get 'converged' than LBM for higher *Ra* number, as the former needs resolving the Poisson's formulation addressing the pressure term [14]. In addition, simulations carried out by Tong and Subramanian[22] were limited to vertical analysis only. Later, the research by Guo and Zhao [11] to study heat transfer through porous media showed interesting comparisons between different techniques, but a firm statement on heat transfer from the horizontal position was still lacking as well as the influence on heat transfer for highly porous medium (e.g., $\mathcal{E}$*=0.9*). The impact of high porosity was numerically evaluated by Zhao et al.[23] and Yao et al. [24] for natural convection considering porous media, and results have not been rehearsed here. Kumar et al. [25] numerically studied a flow of natural convective nature in an enclosed squared porous cavity considering non-linear and inertial influences. This work computationally solved the "dimensionless non-linear coupled partial differential equations" together with suitable sets of boundary conditions with the FDM. Vertical walls had the same temperature and horizontal walls had two dissimilar temperatures and the cavity was inclined at $\gamma = 0^0, 15^0, 45^0, 75^0$ angles. Ameur et al. [26] explored the possibility of reduction of temperature, for cooling purposes, considering "hot shear thinning fluids" flowing throughout a cylinder. CFX code was used to numerically run the simulation. Two techniques, the counter flow and the baffling technique, were explored to figure out the most efficient technique for a cooling process. Changes of flow fields and thermal fields were observed regarding the flow rates and the baffles' pitch ratios. The outcomes demonstrated a big increase in heat transfer rates while implying two strategies at the same time. Sobamowo et al.[27] worked on "magnetohydrodynamic squeezing flow" for nano-fluid considering a porous medium where two parallel plates were implanted in. It was found that if the velocity of the flow rises during the time of squeezing, the *Ha* (Hartmann number) value and squeezing numbers goes downward, yet in the time of separation, the fluid's velocity rises when *Ha* value and squeezing value is increased. Furthermore, an increase in nanofluid's velocity is additionally observed with a rise in

Ha value in a situation of plates moving apart. Still, it was shown that a rise in nanotube concentration causes a rise in the velocity of flow fields at the time of squeezing flow. However, some of the results in the literature do not contain the impact of pore materials in flow physics of the fluid and heat transfer on any physical or computational applications. Most of the numerical studies are limited on fluid flow, heat transfer and velocity profiles, but it is also important to show the extensions of the results for any further applications.

One efficient method to numerically study fluid flow and heat transfer may be established while considering a squared shape or rectangle shape enclosed cavity contained with pore materials. The solid matrix generally employs a tiny bit of an isolated space, yet due to its well built structure, the used surface is large enough to resist the flow. Therefore, the porous layers work as an insulator. A practical application of this particular concept is seen in the indoor heating or cooling system, in this technology the air spaces amongst the wall panels are isolated using light-weight materials like fibreglass[22]. In most of the cases, the enclosures are considered to be filled with porous matrix when insulation is needed. This paper investigates the nature of flow as well as heat transfer through a enclosed cavity which is partially filled with pore materials. From both engineering and mathematical point of views, the purpose is pretty much straightforward. A cavity with partially filled porous material (insulation) will certainly save both the capital and operational costs, considering the fact that the concept of insulation is better optimized.

In this paper, LBM is used to study characteristics of the fluid flow and rate of heat transfer through partially filled porous medium in a squared shape cavity having two dissimilar forms of porous layers namely, horizontally filled porous layer and vertically filled porous layer, at different cases. The simulations were carried out at the REV scale varying Ra values ($Ra = 10^3, 10^4, 10^5, 10^6$), Da values ($Da = 10^{-2}, 10^{-4}$), and, ε values ($\varepsilon = 0.4, 0.6, 0.9$), and average Nu numbers (Nu_{avg}) have been recorded to investigate the patterns and changes of the fluid in terms of flow and heat characteristics. The dependability of the LBM studying heat transfer in porous materials with the Brinkman-Forchheimer mathematical formula has been validated with two sets of numerical simulations. The validation outcomes were observed to be in excellent agreement with some of the benchmark dataset. All the computer simulations are carried out using Fortran 90 code. The computing tool used for these numerical simulations is Fortran PowerStation 4.0. Data sets are generated using this tool and the visualised using Tecplot. The output data sets are studied producing Nu value, Nu_{avg} value, velocity fields, and, contours or isotherm fields along with contours of streamlines.

2. Problem statement and physical geometry

This current work aims to study the flow characteristics and heat transfer characteristics in geometrical formations presented in Fig.1. Figure 1 clearly illustrates the schematic diagram of physical geometry of the design used for this work. This geometry along with the combination of varying Ra values ($Ra = 10^3, 10^4, 10^5, 10^6$), Da values ($Da = 10^{-2}, 10^{-4}$), and, ε values ($\varepsilon = 0.4, 0.6, 0.9$), will present a data set stating the influence of porous media in a free flowing fluid. Since these cavities contain both free flowing fluid zone and partially filled porous zone at the same time, this work will clearly show the characteristic differences in two different zones. The

conductive and convective heat transfer natures, and, the nature of free flowing fluid compared to fluid's flow pattern in the porous zone, are the main focus of this study.

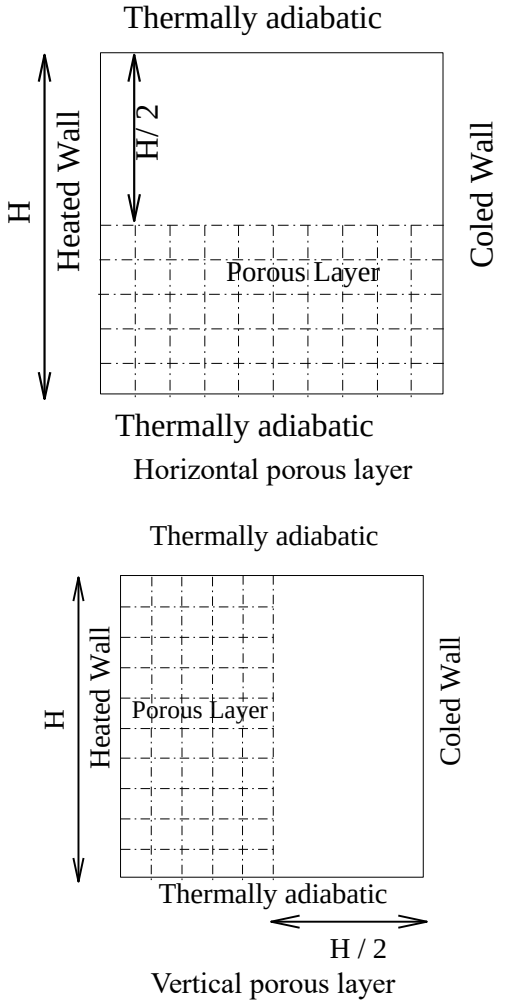

Fig. 1. Schematic diagrams of physical geometry of the design.

The physical geometry of this paper is based on the porosity and insulation property, as discussed in the previous section. The 2D enclosures, considered here are partially filled up containing porous materials. The lattice size of the cavity is *128 × 128*. The investigation of the fluid's flow characteristics through the cavity, and, heat transfer rate characteristics of the enclosed system, has been done from two positions, one having a horizontal porous layer and another having a vertical porous layer. At first, the investigation has been done for a cavity having half-filled horizontal porous layer, as described in Fig. 1(a), where the lower part contains the porous layer. Later, this study was extended to observe the behaviour of the fluid's flow characteristics and heat transfer characteristics in the cavity of the same lattice size, but this time left half of the cavity is considered to contain porous matrix, as shown in Figure 1 (b). In both cases, the left wall of the squared cavity is considered to be hot, and the right wall is considered be cold. Furthermore, upper and lower boundary walls of the enclosures are thermally isolated, that means there are no differences between these two walls.

3. Mathematical formulations

3.1. Lattice boltzmann model

In this work, the mathematical terms of LB method is affiliated with the equation for continuity, the equation for Brinkman-Forchheimer, and the equation for energy transfer. The equations can be described as in the followings [14,21]:

$$\nabla.\bar{u} = 0 \tag{1}$$

$$\partial_t \bar{u} + (\bar{u}.\nabla)\left(\frac{\bar{u}}{\varepsilon}\right) = -\frac{1}{\rho}\nabla(\varepsilon p) + v_e\nabla^2\bar{u} + \bar{F} \tag{2}$$

$$\partial_t T + \nabla.(T\bar{u}) = \alpha\nabla^2 T \tag{3}$$

Where, ε defines porosity of the material, v_e is the effective viscosity, with α being the thermal diffusivity. $\bar{F}$ is the overall body force. The total body force can be defined with the Ergun's relation [28]:

$$\bar{F} = -\frac{\varepsilon v_k}{K}\bar{u} - \frac{1.75}{\sqrt{150\varepsilon K}}|\bar{u}|\bar{u} + \varepsilon\bar{G} \tag{4}$$

Here, v_k represents the kinematic viscosity, K being the permeability, and $\bar{G}$ defines the buoyancy force.

Without the pore materials, Eq. 2 becomes the classical Navier-Stokes equation representing free flows of fluid. The term $v_e\nabla^2\bar{u}$ of Eq. 2 represents the Brinkman component considering the inclusion of a solid materialistic boundary. A thin boundary layer might be used, but can't be negligible for solving mass and heat transfer problems. In addition, the terms $-\frac{\varepsilon v_k}{K}\bar{u}$ and $\frac{1.75}{\sqrt{150\varepsilon K}}|\bar{u}|\bar{u}$ of Eq. 4 respectively represent the linear (Darcy) and non-linear (Forchheimer) drags caused by the inclusion of a pore material. Interestingly, not considering the non-linear component, the whole Eq. 2 is the Brinkman-extended Darcy formulation.

The kinetic equations for two distribution functions namely, f_i and g_i are addressed by the thermal energy distribution LB-method as [29,30]:

$$f_i(x + \bar{e_i}\Delta t, t + \Delta t) - f_i(x,t) = -\frac{f_i(x,t) - f_i^{eq}(x,t)}{\tau_v} + \Delta t F_i \tag{5}$$

$$g_i(x + \bar{e_i}\Delta t, t + \Delta t) - g_i(x,t) = -\frac{g_i(x,t) - g_i^{eq}(x,t)}{\tau_c} \tag{6}$$

Eq. (5) recovers the Eqs. (1-2), and Eq. (6) defines the progress of the internal energy that directs to Equation (3). The macroscopic measures: density of the fluid, velocity as well as temperature can be written as in the followings[31]:

$$\rho = \sum_i f_i \tag{7}$$

$$\bar{u} = \sum_i \frac{\bar{e_i} f_i}{\rho} \tag{8}$$

$$T = \sum_i g_i \tag{9}$$

The equilibrium distribution function regarding the D2Q9 design is[11]:

$$f_i^{eq} = \omega_i \rho \left[1 + \frac{3\bar{e}_i.\bar{u}}{c^2} + \frac{9(\bar{e}_i.\bar{u})^2}{2\varepsilon c^4} - \frac{3\bar{u}^2}{2\varepsilon c^2}\right] \tag{10}$$

Here, ω_i is the weighed factor, and c stands for lattice spacing. In suppose of the D2Q9 design, the discrete velocity components $\bar{e}_i$ have separate values [32]:

$$\bar{e}_0 = 0 \text{ (11a)}$$

$$\bar{e}_i = c\left[\cos(i-1)\frac{\pi}{2}\right];\ i = 1-4 \tag{11b}$$

$$\bar{e}_i = \sqrt{2}c\left[\cos(i-5)\frac{\pi}{2} + \frac{\pi}{4}\right], \left[\sin(i-5)\frac{\pi}{2} + \frac{\pi}{4}\right];\ i = 5-8 \tag{11c}$$

The weighted factors are $\omega_0 = 4/9$, $\omega_i = 1/9$ for *i=1-4*, and $\omega_i = 1/36$ for *i=5-8* [33]. In the same way, the equilibrium distribution function addressing the thermal energy distribution g_i^{eq} is:

$$g_i^{eq} = \omega_i T \left[1 + \frac{3\bar{e}_i.\bar{u}}{c^2} + \frac{9(\bar{e}_i.\bar{u})^2}{2c^4} - \frac{3\bar{u}^2}{2c^2}\right] \tag{12}$$

Other than the proposed forcing term [11,34], an alternative simple forcing term, F_i, is used([13], proposed in this book) for the porous media to get the valid mathematical terms of hydrodynamics by the following relation:

$$F_i = -\omega_i \rho \left[9\frac{\nu}{K}\left(ue_x + ve_y\right) + \frac{\beta}{\sqrt{K}}\left(|\bar{u}|ue_x + |\bar{u}|ve_y\right)\right] \tag{13}$$

Here $\beta = 1.75/\sqrt{150\varepsilon}$. The viscosity ν and thermal diffusivity α can be found from the followings:

$$\nu = \left(\tau_\nu - \frac{1}{2}\right) c_s^2 \Delta t \tag{14}$$

$$\alpha = \left(\tau_c - \frac{1}{2}\right) c_s^2 \Delta t \tag{15}$$

Finally, Darcy number (*Da*) and Rayleigh number can be termed as respectively:

$$Da = \frac{K}{H^2} \qquad and \qquad Ra = \frac{g_0 \beta \Delta T H^3}{\nu\alpha} \tag{16}$$

Here, H is the characteristic length. In the LBM applications, it is important to use *Da* and *Ra* in lattice units, and in that case, H in the Eq. (16) has to be replaced by the quantity of lattices in the considered length direction.

3.2. Boundary condition

In usual cases, for any practical use, macroscopic physical variable terms ρ and $\bar{u}$ are the two main factors used to derive boundary condition. As of the LBM, boundary conditions are simply substituted to distribution function (DF) f_i. Determining distribution functions at boundary nodes

as like the macroscopic boundary conditions is essential in LB-method since this determines both the precision and the stability of the calculation.

3.2.1 Boundary condition for velocity

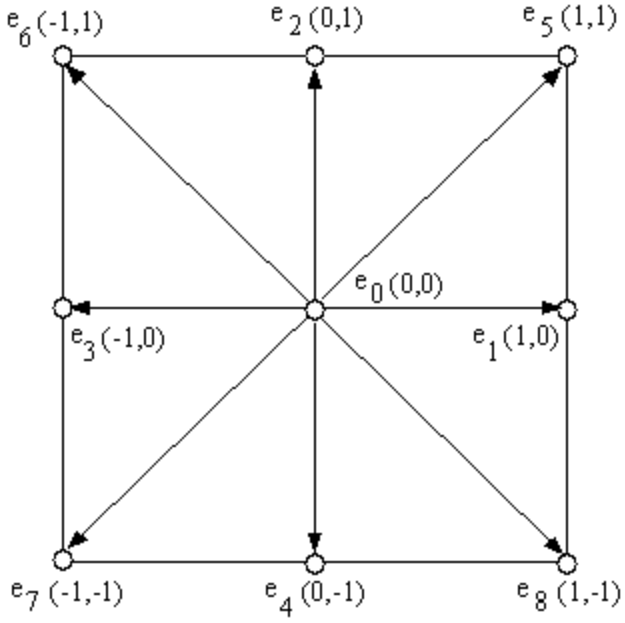

Fig. 2. Discrete velocity vectors in suppose of the *D2Q9* design.

The present approach has been considered in two dimensions, and the boundary conditions are exercised according to *D2Q9* model [13,35,36]. Figure 2 shows the discrete velocity vector descriptions.

No slip boundary conditions are employed at the walls:

Right side (east) wall has the boundary condition of, $f_3 = f_1, f_7 = f_5$ and $f_8 = f_6$.

Left side (west) wall has the boundary condition of, $f_1 = f_3, f_5 = f_7$ and $f_6 = f_8$.

Top side (north) wall has the boundary condition of, $f_4 = f_2, f_7 = f_5$ and $f_8 = f_6$.

South side (bottom) wall has the boundary condition of, $f_2 = f_4, f_5 = f_7$ and $f_6 = f_8$.

3.2.2. Temperatures of the boundary condition

Hot (T_w), cold (Tc) as well as adiabatic temperature conditions are set at the boundary walls.

Right side (east) wall has the cold temperature boundary condition as, $g_3 = Tc\,(W_1 + W_3) - g_1$, $g_7 = Tc\,(W_7 + W_5) - g_5$, together with $g_8 = Tc\,(W_8 + W_6) - g_6$.

At left (west) wall, T_w is used for the 2nd-order Zou-He boundary conditions, which is usually used for the heated wall, and these are $g_1 = T_w\,(W_1 + W_3) - g_3$, $g_7 = T_w\,(W_5 + W_7) - g_5$ and $g_8 = T_w\,(W_8 + W_6) - g_6$

For adiabatic/insulated north (top) wall, the boundary condition is $g_{i,\,n} = g_{i,\,n-1}$

For adiabatic/insulated south (bottom) wall, the boundary conditions is $g_{,i,0} = g_{i,1}$

4. Code validation

Code validation for this thermal LB model is done by performing simulations, and matching average Nusselt number values with two sets of benchmark solutions. In both the validations, simulations of natural convection are restricted inside a *2*-dimensional square enclosure of 128×128 lattice size. The west side wall is hot and the east side wall is cold while the upper and lower walls are kept thermally isolated. For these validation simulations, the entire cavity contains porous materials, and the grid-independent solutions are reported. The generated results are compared with that of the benchmark solutions. For all simulations, the *Pr* value has been set to *1* and Rayleigh number, *Ra*, to 10^3, 10^4, 10^5 and 10^6 are considered.

Table 1
Comparison of the average Nusselt number, present outcomes, with that of the single phase fluid while *Pr* = 0.71.

Ra	***Nu**avg*		
	LBM[14]	FEM [20]	**Present**
10^3	1.117	1.127	1.095
10^4	2.244	2.245	2.245
10^5	4.517	4.521	4.481
10^6	8.758	8.800	8.776

For the first validation, a comparison is illustrated in Table 1 between the average Nusselt numbers of LBM obtained for the range of *Ra* numbers for $\varepsilon = 0.9999$, $Da = 10^7$ and the benchmark data of Seta et al. [14] and FEM study by Nithiarasu et al. [20]. It has been said before that if $\varepsilon \rightarrow 1$ and the *Da* value is high, the equation of the Brinkman-Forchheimer model transform into Navier-Stokes equation of free fluid flows. The numerical values in Table 1 show a good comparative agreement.

The second set of validation data is presented in Table 2. This table compares the average Nusselt numbers of the current LB-Method using the Brinkman-Forchheimer mathematical term together with the predictions of Seta et al. [14], for the Brinkman-Forchheimer formulation and the Brinkman's model of FEM presented by Nithiarasu et al. [20]. Simulations are performed by setting the parametric values to be Da = 10-4, 10-2, Pr = 1 together with ε = 0.4, 0.6, 0.9. The comparative data between the LBM and the FEM is agreeable for the whole range of Da and Ra numbers. It shows that the LB-Method is able to exhibit acceptable resolution for the Brinkman-Forchheimer equation. In addition to numerical data validation of $\mathrm{Nu_{avg}}$, Fig.3 further visualises a comparison of streamline and isotherm contours against the results from Seta et al. [14]. This present LBM work agrees very well with the previous results, generating similar patterns of streamline and isotherm contours.

Table 2
Comparative results against the Brinkman-Forchheimer model at $Pr=1.0$.

Da	Ra	ε	$Nu_{avg}\left(=\frac{1}{H}\int_0^H Nu(y)dy\right)$		
			FEM[20]	LBM [14]	**Present**
10^{-4}	10^5	0.4	1.067	1.063	1.064
		0.6	1.071	1.066	1.068
		0.9	1.072	1.067	1.068
	10^6	0.4	2.55	2.544	2.549
		0.6	2.725	2.610	2.615
		0.9	2.740	2.637	2.636
10^{-2}	10^3	0.4	1.01	1.007	1.009
		0.6	1.015	1.012	1.013
		0.9	1.023	1.017	1.018
	10^4	0.4	1.408	1.362	1.365
		0.6	1.530	1.493	1.495
		0.9	1.64	1.633	1.639
	10^5	0.4	2.983	2.992	2.999
		0.6	3.555	3.433	3.436
		0.9	3.91	3.902	3.909

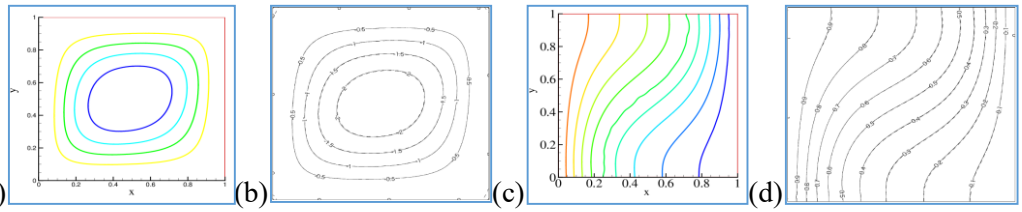

Fig. 3. Comparisons of Streamlines (a) & (b) [14] and Isotherms (c) & (d) [14] contours for $Da = 10^{-2}$, $Ra = 10^4$, and $\varepsilon = 0.6$.

5. Results and discussions

For both horizontal and vertical porous layer analysis, several numerical simulations are performed using the proposed LBM for different iterative combinations by varying *Ra* value, *Da* value and porosity (ε), same procedure is followed for the second part of the code validation. The temperature variation between the west side wall and east side wall causes a buoyancy effect, which is described by the Boussinesq approximation, $G = \beta g_0(T - Tm)\hat{j}$. The generated results show the fluid's flow behaviour through streamlines, isotherms, velocities as well as average Nusselt number.

5.1. Influence on streamlines

Figures 4 (a)-(b) represent the evolution of the streamlines for horizontal porous layer and vertical porous layers, respectively, for all the combinations of the given *Ra*, *Da* and porosity (ε) values. These figures are illustrated using contours of streamlines. The fluid rises in the middle of the cavity due to buoyancy effect and fluid flows upwards along the heated left wall. The top adiabatic wall blocks the flow which then flows along the cold right wall. As a result, re-circulation of fluid is seen within the cavity. A single globular vortex is noticed at the centre of the streamline's contours due to the gravitational and buoyancy effect that are acting opposite to each other inside the cavity. However, in terms of Figure 4 (a), it can be noticed that the

streamline contour lines are more densely packed in the top portion of the cavity than the bottom portion of the cavity, whereas for vertical porous layer in Figure 4(b), this type of scenario can be seen in the rightmost part of the cavity, where the porous materials were considered in the opposite half of the square cavity, this is also seen in the schematic diagram (Figure 1). For simplicity in the explanation, the region where porous matrix is absent has been considered to be "free region", which further can be explained as a zone where fluid flows freely without having any influence of porous layer. In the free region the heat transfer is totally convective whereas the zone containing porous layer shows both convective and conductive heat transfer. More details of the convective and conductive heat transfer phenomenon are discussed later in subsection 6.2. Furthermore, it can be concluded from these figures that the presences of a pore material made a significant influence on the fluid's flow characteristics. In the free flow zone the fluid seems to be flowing smoothly since the distribution of the streamline contours show the fluid has much more presence in the free flowing fluid zone. On the other hand, the zone containing porous media has completely different scenario. In the porous layer zone, the fluid face obstacle to freely flow in the area. This inability of free flow produces comparatively less streamline contours distribution. Hence, it can be concluded that the presence of fluid is comparatively much less in the zone containing porous material. In both cases, porous layers (horizontal or vertical) resist the fluid flow, and hence the fluid tends to flow more towards the free region of the cavity.

5.2. Changes in isotherms

In the observation of fluid's flow characteristics and heat transfer characteristics, isotherm shows whether the pattern of heat transfer has the same characteristics as the conductive heat transfer and convective heat transfer. In the present investigation, changes in isotherm contours have been analysed for considered porous layers, horizontal porous layer and vertical porous layer. Isotherm contours draw a clear picture of the convective heat transfer regions, conductive heat transfer regions, and, mixed convective-conductive heat transfer regions.

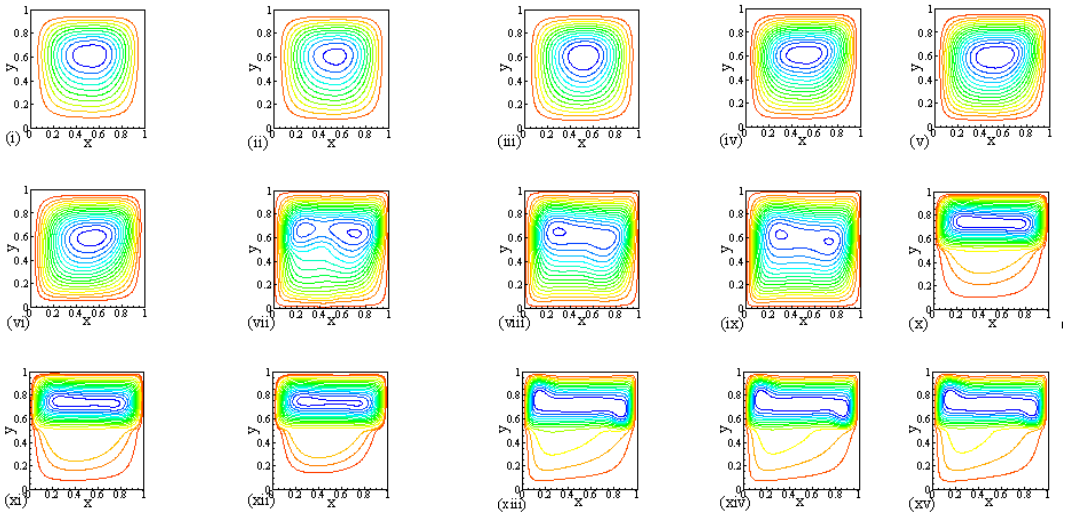

Fig. 4 (a). Streamlines of horizontal porous layer at (i) ε=0.4 (ii) ε=0.6 (iii) ε=0.9 while Ra = 10^3 , Da = 10^{-2}, (iv) ε=0.4 (v) ε=0.6 (vi) ε=0.9 while Ra = 10^4 , Da = 10^{-2}, (vii) ε=0.4 (viii) ε=0.6 (ix) ε=0.9 while Ra = 10^5 , Da = 10^{-2}, (x) ε=0.4 (xi) ε = 0.6 (xii) ε=0.9 while Ra = 10^5 , Da = 10^{-4} and (xiii) ε=0.4 (xiv) ε =0.6 (xv) ε=0.9 while Ra = 10^6 , Da = 10^{-4}.

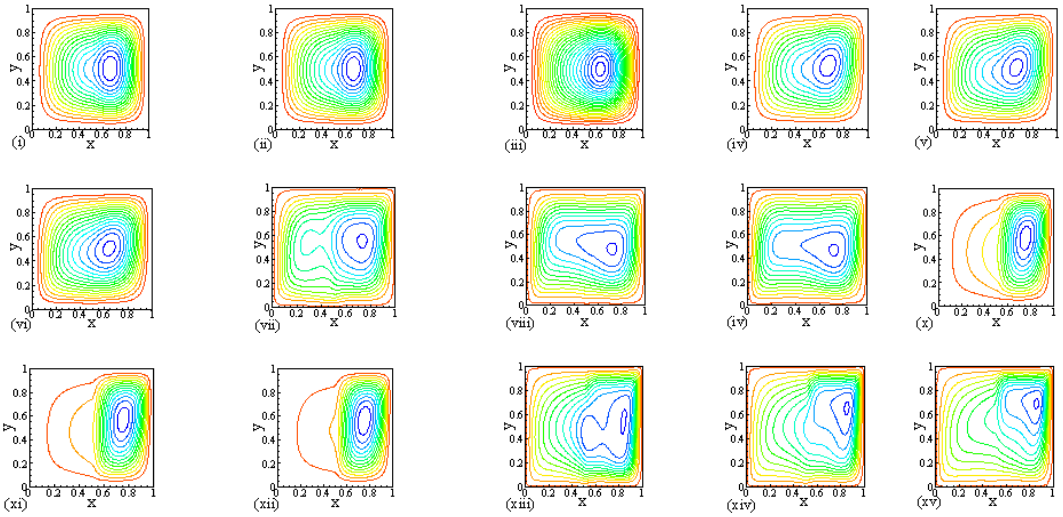

Fig. 4 (b). Streamlines of vertical porous layer at (i) ε=0.4 (ii) ε=0.6 (iii) ε=0.9 while Ra = 10^3 , Da = 10^{-2}, (iv) ε=0.4 (v) ε=0.6 (vi) ε=0.9 while Ra = 10^4 , Da = 10^{-2}, (vii) ε=0.4 (viii) ε=0.6 (ix) ε=0.9 while Ra = 10^5 , Da = 10^{-2}, (x) ε=0.4 (xi) ε=0.6 (xii) ε=0.9 while Ra = 10^5 , Da = 10^{-4} and (xiii) ε=0.4 (xiv) ε =0.6 (xv) ε=0.9 while Ra = 10^6 , Da = 10^{-4}.

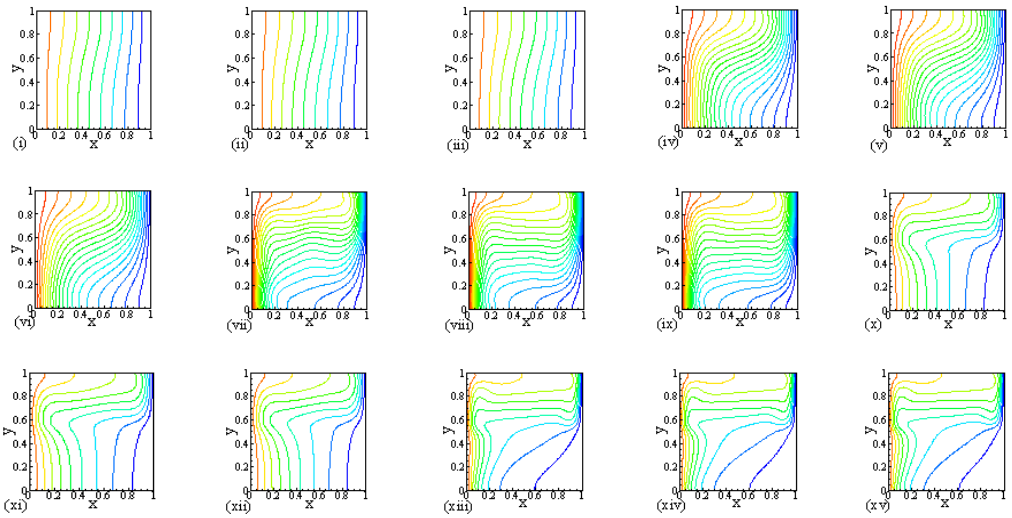

Fig. 5 (a). Isotherms of horizontal porous layer at (i) ε=0.4 (ii) ε=0.6 (iii) ε=0.9 while Ra = 10^3 , Da = 10^{-2}, (iv) ε=0.4 (v) ε=0.6 (vi) ε=0.9 while Ra = 10^4 , Da = 10^{-2}, (vii) ε=0.4 (viii) ε=0.6 (ix) ε=0.9 while Ra = 10^5 , Da = 10^{-2}, (x) ε=0.4 (xi) ε=0.6 (xii) ε=0.9 while Ra = 10^5 , Da = 10^{-4} and (xiii) ε=0.4 (xiv) ε =0.6 (xv) ε=0.9 while Ra = 10^6 , Da = 10^{-4}.

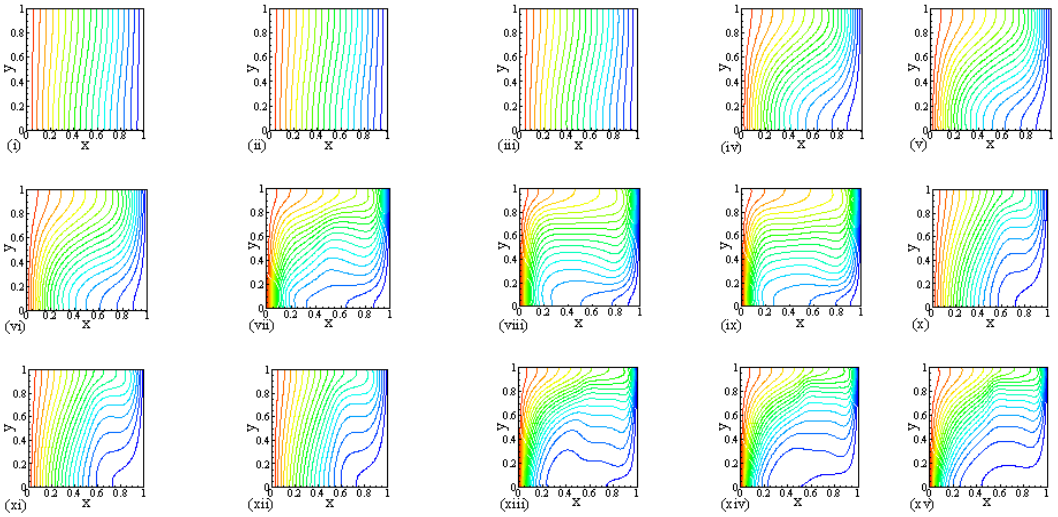

Fig. 5 (b). Isotherms of vertical porous layer at (i) ε=0.4 (ii) ε=0.6 (iii) ε=0.9 while Ra = 10^3 , Da = 10^{-2}, (iv) ε=0.4 (v) ε = 0.6 (vi) ε=0.9 while Ra = 10^4 , Da = 10^{-2}, (vii) ε=0.4 (viii) ε=0.6 (ix) ε=0.9 while Ra = 10^5 , Da = 10^{-2}, (x) ε=0.4 (xi) ε = 0.6 (xii) ε=0.9 while Ra = 10^5 , Da = 10^{-4} and (xiii) ε=0.4 (xiv) ε =0.6 (xv) ε=0.9 while Ra = 10^6 , Da = $10^{-4.}$

In Figures 5 (a) and (b), it is observed that vertical lines are mostly present in the porous regions since heat transfer in this region mostly occurs because of conduction due to the close contacts among the particles. On the other hand, heat transfer in free region takes place through convection as represented by curves in the isotherm plots. Few of the isotherms in Figures 5 (x-xv), possess both vertical and curvy lines in the same plotting frame since the conduction and the convection are occurring simultaneously. This phenomenon is mostly seen during high intensity fluid flow. In addition, it can be concluded from these figures that the presences of a pore material made a significant influence on the heat transfer rate characteristics. In the porous material zone the rate of heat seems to be more since the distribution of the isotherm contours show the contour lines have much more presence in the porous material zone. Conversely, the zone containing no porous media has completely different scenario. In the free fluid zone, the heat transfer rate is comparatively slower. This slow rate of heat transfer produces comparatively less isotherm contours distribution. Hence, it can be concluded that the rate of heat transfer is comparatively much higher in the zone containing porous material.

5.3. Effect of *Ra* and *Da* numbers

Ra value defines the intensification of a fluid flow. For small *Ra* number ($Ra = 10^3$), viscous force shows dominancy over buoyancy force and so the streamlines flow along the geometry of the cavity. This is evident from the streamlines of Figures 4 (i-iii). The temperature profiles, plotted in Figures 5 (i-iii), also show linearity along the x-axis since here heat transfer is taking place pre-dominantly via conduction along the walls of the enclosure and so the isotherms are almost vertical. It can be inferred from this situation that heat transfer mainly takes place due to conduction along the walls of the enclosed cavity. Increasing the *Ra* value to $Ra = 10^4$ intensifies the fluid flow more for which the contour lines of Figures 4 (iv-vi) tend to flow towards and gather around in the non-porous right half of the cavity where it finds more free region to flow.

At this situation, the isotherms in Figures 5 (iv-vi) also seem to bend a little as now heat transfer is occurring through convection. Here, vertical lines are only seen near the hot and cold walls due to thin boundary layers. Further intensifying the fluid flow by increasing Rayleigh number to $Ra = 10^5$ and 10^6 distorts the central globular vortex into an elliptical shape (horizontal) or an oval shape (vertical), which was seen earlier in Figures 4 (vii-ix). The isotherms in Figures 5 (vii-ix) bend into horizontal shape as convection is occurring almost throughout the whole cavity. As the fluid continues to flow, most of the streamlines along with the central vortex get squeezed towards the free region of the cavity where the fluid can flow more freely. Only few streamlines can be observed in the porous layer as the fluid faces more resistance in this region, and thus cannot flow freely. This behaviour is illustrated in Figures 4 (x-xii). Meanwhile, in Figures 5 (x-xv), both vertical lines at porous region and horizontal lines at free region of the cavity are visible in the plots since heat is transferred via both conduction and convection mechanism simultaneously. However, from Figures 4 (xiii-xv), a sudden increase of fluid flow is observed due to increase of Rayleigh number from $Ra = 10^5$ to 10^6 keeping $Da = 10^4$ to be constant.

5.4. Velocity profiles

Figures 6 (a)-(b) show the changes in the *u*-velocity profiles for both horizontal and vertical porous layers, while the trend of *v*-velocities are shown in Fig.7 (a)-(b) regarding the respective cases. These velocities signify the distributions at middle-height of the cavities at dissimilar *Ra* and *Da* values. As *Ra* value increases, the rate of the fluid flow will elevate rapidly in free region. In addition, as the rate of the flow increases, the boundary layer becomes narrower. However, as soon as the flow reaches the porous layers (horizontal or vertical), the flow faces resistance, and hence the velocity reduces significantly, which can be seen at Figures 6 and Figures 7. At the end, the flow velocity will stop once the fluid reaches the porous region. However, with an increase in *Ra* number, the fluid will quickly approach towards the porous media. Hence, the flow velocity will become zero sooner than before.

5.5. Impact of porosity on *Nu* and Nu_{avg}

The Nu_{avg} values presented in this paper are calculated using the following expression:

$$Nu_{avg} = \frac{1}{H}\int_0^H Nu(y).dy \qquad (17)$$

where, *H* is characteristic elevation of the cavity and the $Nu(y) = -\frac{\partial T}{\partial x}$ at $x = 0$.

In computational study of fluid dynamics through porous media, *Da* number defines the effective permeability of the pore material relative to its cross-sectional area. It means when *Da* number decreases, the permeability of the pore material also decreases and vice versa [37]. Figures 8(a)-(b) show the changes in *Nu* numbers for both porous layers. According to Figures 8, when $Da=10^{-2}$, the *Nu* numbers show similar trends for both horizontal and vertical porous layers, as the growth of the heat increases at the commencement. But later, the flow approaches towards the cold wall of the cavity. However, at $Da=10^{-4}$, the *Nu* numbers have very slow growth (horizontal layer), which is because the heat transfer generally depends on conduction. If *Da*

number increases, *Nu* increases rapidly due to the co-existence of convective (natural) and conductive heat transfer in the porous media.

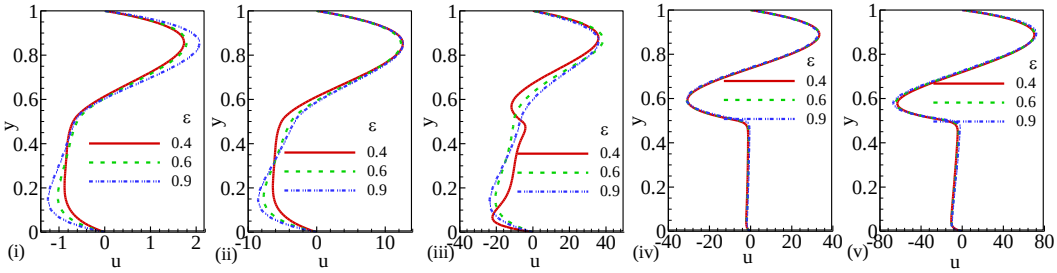

Fig. 6 (a). Effect of porosity parameters on normalized *u* velocity of horizontal porous layer at (i) Ra=10^3, Da=10^{-2}, (ii) Ra=10^4, Da=10^{-2}. (iii) Ra=10^5, Da=10^{-2}, (iv) Ra=10^5, Da=10^{-4} and (v) Ra=10^6, Da=10^{-4}.

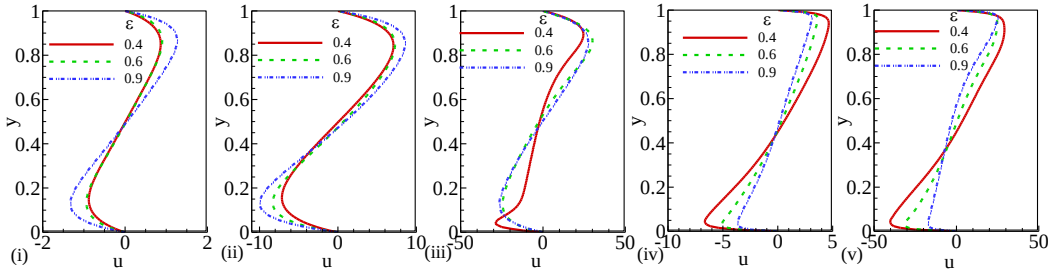

Fig. 6 (b). Effect of porosity parameters on normalized *u* velocity of vertical porous layer at (i) Ra=10^3, = 10^{-2} , (ii) Ra=10^4, Da=10^{-2}. (iii) Ra=10^5, Da=10^{-2}, (iv) Ra=10^5, Da=10^{-4} and (v) Ra=10^6, Da=10^{-4}.

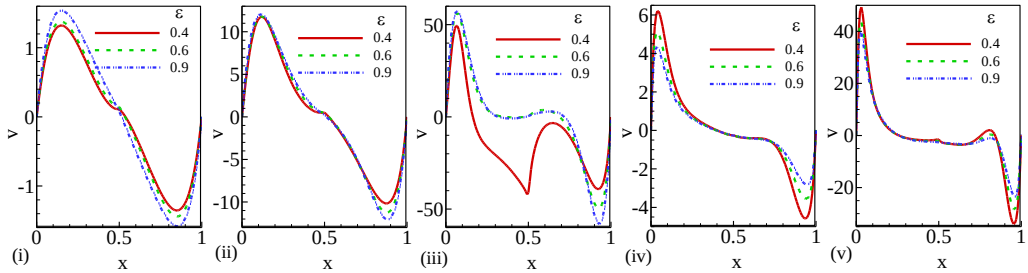

Fig. 7 (a). Effect of porosity parameters on normalized *v* velocity of horizontal porous layer at (i) Ra=10^3, Da=10^{-2}, (ii) Ra=10^4, Da=10^{-2}. (iii) Ra=10^5, Da=10^{-2}, (iv) Ra=10^5, Da=10^{-4} and (v) Ra=10^6, Da=10^{-4}.

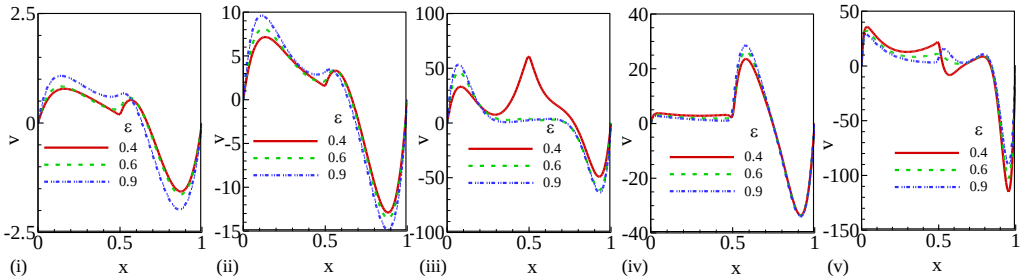

Fig. 7 (b). Effect of porosity parameters on normalized *v* velocity of vertical porous layer at (i) Ra=10^3, $Da = 10^{-2}$, (ii) Ra=10^4, Da=10^{-2}. (iii) Ra=10^5, Da=10^{-2}, (iv) Ra=10^5, Da=10^{-4} and (v) Ra=10^6, Da=10^{-4}.

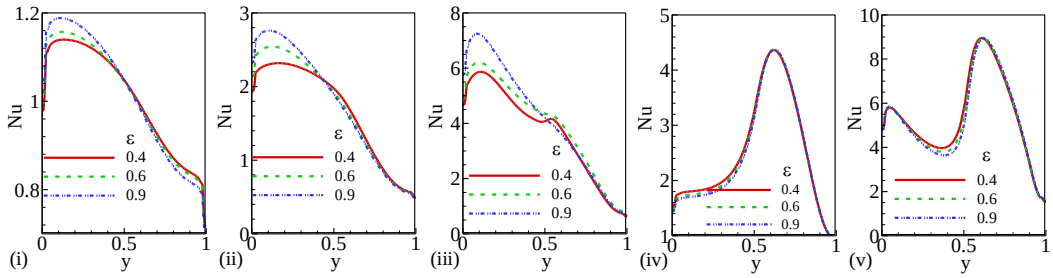

Fig. 8 (a). Influence of porosity parameters on *Nu*, of horizontal porous layer at (i) $Ra=10^3$, $Da=10^{-2}$, (ii) $Ra=10^4$, $Da=10^{-2}$. (iii) $Ra=10^5$, $Da=10^{-2}$, (iv) $Ra=10^5$, $Da=10^{-4}$ and (v) $Ra=10^6$, $Da=10^{-4}$.

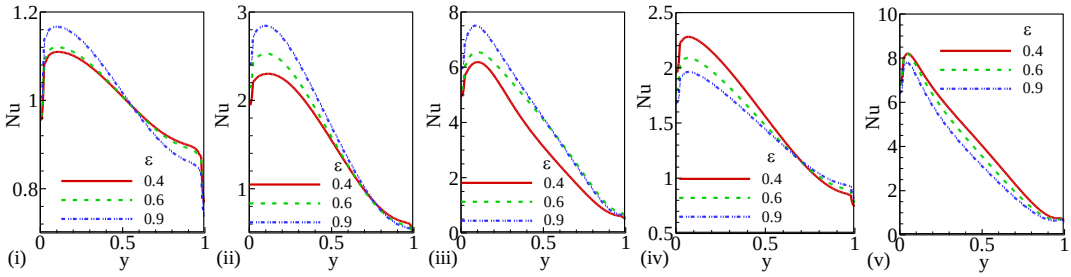

Fig. 8(b). Influence of porosity parameters on *Nu*, of vertical porous layer at (i) $Ra=10^3$, $Da=10^{-2}$, (ii) $Ra=10^4$, $Da=10^{-2}$. (iii) $Ra=10^5$, $Da=10^{-2}$, (iv) $Ra=10^5$, $Da=10^{-4}$ and (v) $Ra=10^6$, $Da=10^{-4}$.

Influence of ε value on the convective heat transfer for fixed *Ra* and *Da* values for cases of horizontal and vertical layer of pore materials is demonstrated in Fig. 8 (a)-(b) and Table 3. The generated results illustrate that the rate of heat transfer gets slower as porosity increases. For given *Ra* and *Da* values, a higher porosity means lower contact surface area between the particles and less resistance for fluid flow, thereby minimising the heat transfer mechanism. In other words, as porosity decreases, the *Nu* number increases for both horizontal and vertical porous layers. Considering the numerical data in Table 3, it is observed that at $Da=10^{-4}$ and $Ra=10^5$, if the porosity reduces from *0.9* to *0.6* (difference of only *0.3*), the average *Nu* number increases by *0.03* unit (horizontal) and *0.05* unit (vertical). In case the porosity reduction is almost doubled (i.e. by *0.5* unit) from *0.9* to *0.4*, average *Nu* value rises by *0.06* and *0.13* units for horizontal and vertical porous layers, respectively. It can be deduced that heat transfer gets doubled as reduction of porosity is doubled, although the variation of porosity affects the average *Nu* number slightly since *Da* number is low. This pattern is also evident if *Ra* number is increased to 10^6 keeping *Da* number as 10^{-4}. Therefore, it can be anticipated that *Nu* numbers will gradually reach the maximum value as the porosity continues to decrease significantly making the particles more compacted. However, the above mentioned criterion does not hold in case of low *Ra* and *Da* numbers. At $Da=10^{-2}$ and $Ra=10^3$ and 10^4, decrease in porosity has almost no impact on the rate of heat transfer, that is, the Nu_{avg} values are not affected by porosity ($\mathcal{E}$), *Ra* or *Da* numbers when *Ra* and *Da* numbers are low. Table 3 also depicts the fact that at $Ra=10^5$ and $Da=10^{-2}$, change in porosity has great impact on natural convective heat transfer [24]. Here, as porosity is increased from *0.4* to *0.9*, the Nu_{avg} value also gets higher significantly (by *0.45* units for horizontal and *0.84* units for vertical) due to increase in permeability. Furthermore, it is observed from the tabulated results that, for same amount of porosity variation, changes in average *Nu* number for vertical porous layer is more than that of

horizontal layer. Therefore, it can be inferred that insulating an enclosed area vertically will be a better option than doing it horizontally.

The ability of the current LB-method to exhibit the solutions of Brinkman-Forchheimer formulation correctly has already been proven and validated using Table 1 and Table 2. After simulating for horizontal and vertical porous layer, the Nu_{avg} values are tabulated in Table 3. The experimental data of the LBM solutions can predict the non-Darcy behaviour accurately. This can be comprehended from the trend of the data in all the tables, as well as, in the simulation plots:

If the *Da* and *Ra* numbers are fixed, the average *Nu* number increases with porosity almost linearly.

If the *Da* and porosity (Ɛ) are fixed, then higher *Ra* value results in the average *Nu* value to get high.

If the *Ra* number and Ɛ are fixed, the Nu_{avg} increases with a higher value of *Da* because of increasing permeability of the pore material that speeds up the flow velocity of the fluid.

If the *Da* and *Ra* numbers are low, the average *Nu* numbers are not affected by porosity (Ɛ), *Ra* or *Da* numbers.

The *Da* and *Ra* numbers have considerable influence on fluid flow and rate of heat transfer, of which the latter affect more distinctly than the former. Moreover, at high *Da* number, the natural convective heat transfer in enclosed cavity enhance significantly as the porosity increases.

Table 3
Numerical results of Nu_{avg} for both horizontal and vertical porous layers.

Da	***Ra***	Nu_{avg}					
		$\mathcal{E}$**= 0.4**		$\mathcal{E}$**= 0.6**		$\mathcal{E}$**= 0.9**	
		Horizontal	**Vertical**	**Horizontal**	**Vertical**	**Horizontal**	**Vertical**
10^{-4}	10^5	2.505038	1.568069	2.477976	1.490630	2.453791	1.447912
	10^6	5.401911	4.141382	5.334390	3.843745	5.282199	3.486232
10^{-2}	10^3	1.015100	1.006989	1.017237	1.008230	1.022974	1.016320
	10^4	1.684465	1.511022	1.729577	1.582478	1.776947	1.713148
	10^5	3.722578	3.300134	3.992295	3.910919	4.168695	4.136219

6. Conclusion

LBM had been used to numerically study fluid flow and heat transfer considering a pore material at REV scale inside a square enclosure. Brinkman-Forchheimer equation was incorporated in the present non-Darcy system to deliberate both inertial and viscous terms. The adaptability of LBM with Brinkman-Forchheimer equation was validated with benchmark results and was found to be in good agreement. Compared to the conventional FEM, LBM was found to be numerically more accurate with less time-scale to complete the simulation task. Simulation results obtained by the present LB model could provide details of the nature of the flow in different geometrical alignments. The results also conclude that not only porosity of the medium is responsible to influence the fluid flow and the rate of heat transfer in the theory of fluid dynamics, but also the

dimensionless parameters like *Ra* number and *Da* number play vital role. When *Ra* and *Da* numbers were kept constant, the rate of heat transfer, defined by Nu_{avg}, increased with porosity. Rate of heat transfer also showed increment for fixed porosity values and *Da* value. Enhancing the permeability of the porous medium by increasing *Da* number also helped to improve the rate of heat transfer. However, no impact of the dimensionless parameters and porosity could be seen on the Nu_{avg} for lower *Da* and *Ra* values. These properties are the behaviours of the non-Darcian flow which were successfully obtained numerically through the present LBM solutions.

Nomenclature

English symbols

c	lattice spacing
Da	Darcy number
e_i	discrete velocity
$\bar{F}$	total body force
f_i	velocity distribution function
$\bar{G}$	buoyancy force
g_i	thermal distribution function
g_0	acceleration due to gravity
H	characteristic length
$\hat{j}$	unit vector in y-direction
Nu	local Nusselt number
Nu_{avg}	average Nusselt number
Pr	Prandtl number
p	pressure
K	permeability
Ra	Rayleigh number
T	fluid temperature
$\bar{u}$	fluid velocity
v	normalized velocity
W	block separation distance
x, y	cartesian co-ordinates

Greek symbols

α	thermal diffusivity
β	volumetric expansion co-efficient
Σ	summation operator
Δ	delta operator
∇	divergence operator
∂	differential operator
ε	porosity
ρ	fluid density
τ	single relaxation time
ω_i	weighted factor
ν	kinematic viscosity

Subscripts

c	cold
e	effective
k	kinematic
m	mean
s	speed
t	time
w	hot

Superscripts

eq	equilibrium

References

[1] Douglas, Jr. J. Finite Difference Methods for Two-Phase Incompressible Flow in Porous Media. SIAM J Numer Anal 1983;20:681–96. doi:10.1137/0720046.

[2] Kim J-G, Deo MD. Finite element, discrete-fracture model for multiphase flow in porous media. AIChE J 2000;46:1120–30. doi:10.1002/aic.690460604.

[3] Jenny P, Lee SH, Tchelepi HA. Adaptive Multiscale Finite-Volume Method for Multiphase Flow and Transport in Porous Media. Multiscale Model Simul 2005;3:50–64. doi:10.1137/030600795.

[4] Zarghami A, Ubertini S, Succi S. Finite volume formulation of thermal lattice Boltzmann method. Int J Numer Methods Heat Fluid Flow 2014.

[5] Radu FA, Nordbotten JM, Pop IS, Kumar K. A robust linearization scheme for finite volume based discretizations for simulation of two-phase flow in porous media. J Comput Appl Math 2015;289:134–41.

[6] Javandel I, Witherspoon PA. Application of the finite element method to transient flow in porous media. Soc Pet Eng J 1968;8:241–52.

[7] Khoei AR, Hosseini N, Mohammadnejad T. Numerical modeling of two-phase fluid flow in deformable fractured porous media using the extended finite element method and an equivalent continuum model. Adv Water Resour 2016;94:510–28.

[8] Balasubramanian K, Hayot F, Saam WF. Darcy's law from lattice-gas hydrodynamics. Phys Rev A 1987;36:2248–53. doi:10.1103/PhysRevA.36.2248.

[9] Rothman DH. Cellular-automaton fluids: A model for flow in porous media. GEOPHYSICS 1988;53:509–18. doi:10.1190/1.1442482.

[10] Mosthaf K, Helmig R, Or D. Modeling and analysis of evaporation processes from porous media on the REV scale. Water Resour Res 2014;50:1059–79. doi:10.1002/2013WR014442.

[11] Guo Z, Zhao TS. Lattice Boltzmann model for incompressible flows through porous media. Phys Rev E 2002;66:036304. doi:10.1103/PhysRevE.66.036304.

[12] Chen S, Doolen GD. LATTICE BOLTZMANN METHOD FOR FLUID FLOWS. Annu Rev Fluid Mech 1998;30:329–64. doi:10.1146/annurev.fluid.30.1.329.

[13] Mohamad AA. Lattice Boltzmann Method. vol. 70. Springer; 2011.

[14] Seta T, Takegoshi E, Okui K. Lattice Boltzmann simulation of natural convection in porous media. Math Comput Simul 2006;72:195–200. doi:10.1016/j.matcom.2006.05.013.

[15] Whitaker S. The Forchheimer equation: A theoretical development. Transp Porous Media 1996;25:27–61. doi:10.1007/BF00141261.

[16] Huang H, Ayoub JA. Applicability of the Forchheimer Equation for Non-Darcy Flow in Porous Media. SPE Annu. Tech. Conf. Exhib., Society of Petroleum Engineers; 2006. doi:10.2118/102715-MS.

[17] Durlofsky L, Brady JF. Analysis of the Brinkman equation as a model for flow in porous media. Phys Fluids 1987;30:3329. doi:10.1063/1.866465.

[18] Nishad CS, Chandra A, Karmakar T, Raja Sekhar GP. A non-primitive boundary element technique for modeling flow through non-deformable porous medium using Brinkman equation. Meccanica 2018;53:2333–52. doi:10.1007/s11012-018-0832-4.

[19] Lauriat G, Prasad V. Non-Darcian effects on natural convection in a vertical porous enclosure. Int J Heat Mass Transf 1989;32:2135–48. doi:10.1016/0017-9310(89)90120-8.

[20] Nithiarasu P, Seetharamu KN, Sundararajan T. Natural convective heat transfer in a fluid saturated variable porosity medium. Int J Heat Mass Transf 1997;40:3955–67. doi:10.1016/S0017-9310(97)00008-2.

[21] Haghshenas A, Nasr MR, Rahimian MH. Numerical simulation of natural convection in an open-ended square cavity filled with porous medium by lattice Boltzmann method. Int Commun Heat Mass Transf 2010;37:1513–9. doi:10.1016/j.icheatmasstransfer.2010.08.006.

[22] Tong TW, Subramanian E. Natural convection in rectangular enclosures partially filled with a porous medium. Int J Heat Fluid Flow 1986;7:3–10. doi:10.1016/0142-727X(86)90033-0.

[23] Zhao CY, Dai LN, Tang GH, Qu ZG, Li ZY. Numerical study of natural convection in porous media (metals) using Lattice Boltzmann Method (LBM). Int J Heat Fluid Flow 2010;31:925–34. doi:10.1016/j.ijheatfluidflow.2010.06.001.

[24] Yao S-G, Duan L-B, Ma Z-S, Jia X-W. The Study of Natural Convection Heat Transfer in a Partially Porous Cavity Based on LBM. Open Fuels Energy Sci J 2014;7:88–93. doi:10.2174/1876973X01407010088.

[25] Kumar V, Rani A, Singh AK. Numerical solution of non-Darcian effects on natural convection in a rectangular inclined porous enclosure with heated walls, 2019, p. 020107. doi:10.1063/1.5135282.

[26] Ameur H, Kamla Y, Sahel D. Numerical investigation of the cooling of shear thinning fluids in cylindrical horizontal ducts. Comput Eng Phys Model 2018;1:54–64.

[27] Sobamowo GM, Jayesimi O, Waheed A. On the study of magnetohydrodynamic squeezing flow of nanofluid between two parallel plates embedded in a porous medium. Comput Eng Phys Model 2018;1:1–15.

[28] Ergun S. Fluid flow through packed columns. Chem Eng Prog 1952;48:89–94.

[29] Peng Y, Shu C, Chew YT. Simplified thermal lattice Boltzmann model for incompressible thermal flows. Phys Rev E 2003;68:026701. doi:10.1103/PhysRevE.68.026701.

[30] Himika TA, Hasan M, Molla M. Lattice Boltzmann simulation of airflow and mixed convection in a general ward of hospital. J Comput Eng 2016;2016.

[31] Hasan MF, Himika TA, Molla MM. Large-eddy simulation of airflow and heat transfer in a general ward of hospital, 2016, p. 050022. doi:10.1063/1.4958413.

[32] Gao C, Xu R-N, Jiang P-X. Pore-scale numerical investigations of fluid flow in porous media using lattice Boltzmann method. Int J Numer Methods Heat Fluid Flow 2015;25:1957–77. doi:10.1108/HFF-07-2014-0202.

[33] Amine Moussaoui M, Jami M, Mezrhab A, Naji H. Computation of heat transfer and fluid flow in an obstructed channel using lattice Boltzmann method. Eng Comput 2010;27:106–16. doi:10.1108/02644401011008540.

[34] Guo Z, Zhao TS. A LATTICE BOLTZMANN MODEL FOR CONVECTION HEAT TRANSFER IN POROUS MEDIA. Numer Heat Transf Part B Fundam 2005;47:157–77. doi:10.1080/10407790590883405.

[35] Guo Y, Bennacer R, Shen S, Ameziani DE, Bouzidi M. Simulation of mixed convection in slender rectangular cavity with lattice Boltzmann method. Int J Numer Methods Heat Fluid Flow 2010;20:130–48. doi:10.1108/09615531011008163.

[36] Hasan M, Ahmed Himika T, Molla M. Lattice Boltzmann simulation of airflow and heat transfer in a model ward of a hospital. J Therm Sci Eng Appl 2017;9.

[37] Vafai K. Handbook of porous media, Crc Press, 2015 n.d.